

Oscillations of vertically integrated relativistic tori – I. Axisymmetric modes in a Schwarzschild spacetime

Luciano Rezzolla^{(1),(2)}, Shin’ichirou Yoshida⁽¹⁾ and Olindo Zanotti⁽¹⁾

¹*SISSA, International School for Advanced Studies, Via Beirut, 2 34014 Trieste, Italy*

²*INFN, Sezione di Trieste, Via Valerio, 2 34127 Trieste, Italy*

3 December 2018

ABSTRACT

This is the first of a series of papers investigating the oscillation properties of relativistic, non-selfgravitating tori orbiting around a black hole. In this initial paper we consider the axisymmetric oscillation modes of a torus constructed in a Schwarzschild spacetime. To simplify the treatment and make it as analytical as possible, we build our tori with vertically integrated and vertically averaged quantities, thus transforming the eigenvalue problem into a set of coupled ordinary differential equations. The tori are also modeled with a number of different non-Keplerian distributions of specific angular momentum and we discuss how the oscillation properties change when different distributions of angular momentum are considered. Our investigation progresses by steps. We first consider a local analysis in Newtonian gravity and determine the properties of acoustic wave propagation within these objects, as well as the relations between acoustic and epicyclic oscillations. Next, we extend the local analysis to a general relativistic framework. Finally, we perform a global analysis and determine both the eigenfunctions and the eigenfrequencies of the axisymmetric oscillations corresponding to the p modes of relativistic tori. These behave as sound waves globally trapped in the torus and possess eigenfrequencies appearing in the simple sequence 2:3:4:..., independently of the distribution of angular momentum considered. The properties of the modes investigated here are in good agreement with those observed in recent numerical simulations and could have a number of different applications. In X-ray binary systems containing a black hole candidate, for instance, p -mode oscillations could be used to explain the harmonic relations in the high frequency quasi-periodic oscillations observed. In systems comprising a massive torus orbiting a black hole, on the other hand, p -mode oscillations could be used to explain the development or the suppression of the runaway instability.

Key words: accretion discs – general relativity – hydrodynamics – oscillations

1 INTRODUCTION

Waves and normal-mode oscillations in stars have long since attracted attention and a vast literature, investigating them both in Newtonian (see, for instance, Cox 1980, or Unno et al., 1989) and in general relativistic regimes (see Stergioulas 1998, for a review), is now available. On the other hand, waves and normal-mode oscillations in geometrically thin discs around compact objects have been studied much less, both within Newtonian gravity (see Kato 2001 for a review) and within a relativistic framework (Okazaki et al., 1987; Perez et al., 1997; Silbergleit et al., 2001; Kato 2001, Rodriguez et al. 2002). The literature is even more scarce when one considers geometrically thick discs, which so far have been investigated mostly in connection with their stability properties both in Newtonian gravity (Papaloizou and Pringle 1984, 1985; Blaes 1985) and in general relativity (Kojima, 1986). An explanation for why discoseismology has not yet reached the development and the level of sophistication which is now possible in asteroseis-

mology is due, at least in part, to the fact that only recently accretion discs have been recognized as fundamental astrophysical objects, present in various forms at all scales. Nowadays, however, periodic and quasi-periodic variations are currently observed in different classes of astrophysical objects containing accretion discs. Although many different models have been proposed for the interpretation of the rich phenomenology associated with these quasi-periodic oscillations (QPOs), there seems not to be yet a widely accepted mechanism for most of the observed sources (see van der Klis, 2000 for a review). Clearly, a systematic investigation of the oscillation properties of discs could shed some light on this.

As in stars, oscillation modes in discs are, in general, the consequence of restoring forces responding to perturbations and these offer a way for classifying oscillations. In accretion discs, in particular, a first restoring force is given by the centrifugal force, which is responsible for the appearance of the so called *inertial waves*, tightly related to the orbital motion of the disc and hence to

epicyclic oscillations. A second restoring force is offered by pressure gradients and the oscillations that are produced in this way are related to p modes and have close connections with the propagation of *sound waves* in the perturbed fluid. A third restoring force is the gravitational field in the direction orthogonal to the orbital plane. If a portion of the disc is perturbed in the vertical direction, in fact, the vertical component of the gravitational field will produce a harmonic oscillation across the equatorial plane with oscillation frequency equal to the orbital frequency. These oscillations are related to *corrugation waves* (see Kato, Fukue and Mineshige, 1998, for an overview on disc oscillations).

Two complementary approaches have been followed traditionally for studying the perturbations of equilibrium models of geometrically thin accretion discs. The first one is a *local* approach, and it has been used extensively to investigate the propagation of waves with the inclusion of many contributing physical effects, such as buoyancy, stratified atmospheres and magnetic fields (see, among the others, Lubow and Ogilvie, 1998). Being local, these approaches derive dispersion relations in which the frequency of the perturbation is expressed as a function of the spatial position within the object and as the linear combination of different contributions, each related to the different physical effect (Kato, 2001). The second approach is a *global* one and it is based on the fact that, under suitable conditions, Eulerian perturbations to all physical quantities can be expressed as an eigenvalue problem, the eigenvalue being the frequency of oscillation. In practice, and for the simplest case, this amounts in solving a second order partial differential equation once appropriate boundary conditions are provided (see Ipser and Lindblom, 1992; Silbergleit et al., 2001; Nowak and Wagoner, 1991).

This paper is devoted to both a local and a global perturbative analysis of axisymmetric modes of oscillation of relativistic tori in the Cowling approximation (i.e. in an approximation in which the perturbations of the spacetime are neglected; Cowling 1941). Fluid tori differ from geometrically thin discs mostly in having equilibrium configurations in which the orbital motion is intrinsically non-Keplerian and in which pressure gradients play an important role, giving rise to an extended vertical structure. As a result, a consistent investigation of these configurations which would account for the coupling of the oscillations in the radial and vertical directions requires necessarily a two-dimensional treatment involving a set of partial differential equations. While this problem is solvable with presently available techniques (this has indeed already been done for relativistic rotating stars; Yoshida and Eriguchi, 1997), it would require a massive use of expensive numerical calculations leaving little room to a physical interpretation. Furthermore, in contrast with the case of relativistic stars, the eigenvalue problem for relativistic tori is in great part unsolved and resorting to a fully numerical solution at this stage would prevent one from appreciating most of the basic physics behind the oscillation modes of these objects. For this reason, we will here concentrate on a simpler model for the torus which can be handled in great part analytically, and postpone the use of the two-dimensional fully numerical analysis to a subsequent work.

The main simplification in the models discussed here is that the vertical structure of the tori is accounted for by integrating the relevant quantities along the direction perpendicular to the equatorial plane. Doing so removes one spatial dimension from the problem, which can then be solved integrating simple ordinary differential equations. The local approach, in particular, will allow us to derive the local dispersion relation obeyed by the oscillations in

relativistic non-Keplerian discs, while the global approach will provide us with the eigenfunctions and eigenfrequencies of the system.

There are several motivations behind this study. Firstly, we want to extend the relativistic discoseismology analysis carried so far for thin discs to systems having a non negligible contribution coming from pressure gradients. Secondly, we intend to interpret and clarify some of the numerical results found in the time evolution of “toroidal neutron stars”, i.e. compact and massive tori orbiting a Schwarzschild black hole (Zanotti, Rezzolla & Font, 2003). Thirdly, we want to assess the possible connections between the oscillation modes of relativistic tori and the rich X-ray phenomenology observed in QPOs. Finally, we want to investigate the possibility that the axisymmetric oscillations of thick discs could provide a criterion for the development or the suppression of the runaway instability (Abramowicz et al., 1983).

The plan of the paper is as follows: in Section 2 we briefly review the local analysis of oscillation modes in vertically integrated Newtonian tori. Section 3, on the other hand, introduces the basic assumptions and equations employed in the definition of our general relativistic, vertically integrated torus. These equations will then be used to study axisymmetric oscillations both locally, in Section 4, and globally, in Section 5. We will first consider configurations with constant distributions of specific angular momentum, and subsequently distributions of specific angular momentum that are either linear or power-laws in the cylindrical radial coordinate. Finally, Section 8 contains our conclusions and the prospects for further investigations. Hereafter Greek indices are taken to run from 0 to 3 and Latin indices from 1 to 3; unless stated differently, we will use units in which $G = c = M_{\odot} = 1$.

2 NEWTONIAN TORI: A LOCAL ANALYSIS

We here briefly present a local analysis of the oscillation modes of vertically integrated tori within a Newtonian framework. Some of the results presented in this Section have already been discussed in the literature, but will serve as a useful reference for the general relativistic treatment presented in Section 4, and will help in the physical interpretation of the relativistic results.

2.1 Assumptions and Equations

Consider an extended perfect fluid configuration orbiting a central object which is the only source of the gravitational potential (i.e. the orbiting fluid is non-selfgravitating). Introduce now a cylindrical coordinate system, (ϖ, ϕ, z) whose origin is at the center of the central object and whose z -axis is oriented along the direction of the orbital angular momentum vector.

A simplified description of this system can be obtained by removing the dependence of the various physical quantities on the vertical coordinate z . Mathematically, this is done by integrating the relevant physical quantities along the vertical direction. Physically, this corresponds to collapsing the vertical structure of the torus onto the equatorial plane, but is quite *different* from just considering an equatorial slice of the vertically extended torus.

Using this approach, it is possible to define the *vertically integrated* pressure P

$$P(\varpi) \equiv \int_{-H}^H p dz, \quad (1)$$

and the vertically integrated rest-mass density Σ

$$\Sigma(\varpi) \equiv \int_{-H}^H \rho dz, \quad (2)$$

where $H = H(\varpi)$ is the local “thickness” of the torus. An equation of state (EOS) for the fluid in the torus needs to be specified and we find it convenient to use here a simple barotropic EOS of polytropic type, i.e.

$$p = k\rho^\gamma, \quad (3)$$

where k and $\gamma \equiv d \ln p / d \ln \rho$ are the polytropic constant and the adiabatic index, respectively. The vertically integrated quantities in (1) and (2) need also to be related through an “effective” equation of state and this can be done if we define an “effective” adiabatic index $\Gamma \equiv d \ln P / d \ln \Sigma$, so that

$$P = \mathcal{K} \Sigma^\Gamma, \quad (4)$$

with the constants \mathcal{K} and Γ playing the role of the polytropic constant and of the adiabatic index, respectively. Note that while equation (4) mimics a polytropic equation of state, it does not represent a vertically integrated polytropic equation of state (unless, of course, the adiabatic index is equal to one). More importantly, the adiabatic index Γ is *not* constant but depends both on ϖ and z . This complication, however, can be removed if one assumes that both the pressure and the rest-mass density have a weak dependence on height, so that they can be accurately expressed in terms of their values at the equator, i.e.

$$p = p(\varpi, z) \approx p_0 \equiv p(\varpi, z = 0), \quad (5)$$

$$\rho = \rho(\varpi, z) \approx \rho_0 \equiv \rho(\varpi, z = 0). \quad (6)$$

Using this assumption, $P \approx 2H p_0$ and $\Sigma \approx 2H \rho_0$, so that $\Gamma \approx d \ln p_0 / d \ln \rho_0 = \gamma$ and equation (4) can effectively be written as

$$P = k \Sigma^\gamma. \quad (7)$$

In all of the calculations reported here we have used $\Gamma = 4/3$, but the results do not change qualitatively when different polytropic indices are used.

Being in circular non-Keplerian motion with angular velocity Ω , the torus will have velocity components only in the ϖ and in the ϕ -directions, with *vertical averages* given by

$$U(\varpi) \equiv \frac{1}{2H} \int_{-H}^H v^\varpi dz, \quad (8)$$

and

$$W(\varpi) \equiv \frac{1}{2H} \int_{-H}^H v^\phi dz. \quad (9)$$

With these assumptions, the dynamics of the torus is fully described by a set of equations comprising the Euler equations in the ϖ and ϕ -directions (Shu, 1992)

$$\partial_t U + U \partial_\varpi U + \frac{W}{\varpi} \partial_\phi U - \frac{W^2}{\varpi} = -\frac{1}{\Sigma} \partial_\varpi P - \partial_\varpi \Psi, \quad (10)$$

$$\begin{aligned} \partial_t W + U \partial_\varpi W + \frac{W}{\varpi} \partial_\phi W + \frac{UW}{\varpi} = \\ -\frac{1}{\Sigma} \frac{1}{\varpi} \partial_\phi P - \frac{1}{\varpi} \partial_\phi \Psi, \end{aligned} \quad (11)$$

the equation for the conservation of mass

$$\partial_t \Sigma + \partial_\varpi (\Sigma U) + \frac{1}{\varpi} \Sigma U + \frac{1}{\varpi} \partial_\phi (\Sigma W) = 0, \quad (12)$$

and the Poisson equation for a vertically integrated gravitational potential Ψ

$$\nabla^2 \Psi = 4\pi \mathcal{S}, \quad (13)$$

where \mathcal{S} is the vertically integrated rest-mass density of the central object, only source of the gravitational potential.

Stationary and axisymmetric models for the tori can be built after setting to zero the terms in (10)–(12) involving derivatives with respect to the t and ϕ -coordinates. The solutions obtained in this way represent the background equilibrium solutions over which harmonic Eulerian perturbations of the type

$$\begin{pmatrix} \delta U \\ \delta W \\ \delta q \end{pmatrix} \sim e^{-i\sigma t + ik_\varpi \varpi}, \quad (14)$$

can be introduced. Note that Eulerian perturbations are indicated with a “ δ ” to distinguish them from the corresponding Lagrangian perturbations, that we will instead indicate with a “ Δ ”. In expression (14), σ is the frequency of the perturbation (in general a complex number), k_ϖ is the wavenumber in the ϖ -direction (hereafter simply k), and $\delta q \equiv \delta P / \Sigma$ has been introduced to describe the perturbation in the pressure.

We have here neglected the perturbations in the gravitational potential and therefore set $\delta \Psi = 0$. This is referred to as the Cowling approximation (Cowling 1941) and for a fluid configuration which is non-selfgravitating (i.e. one whose gravitational potential is such that $\Psi_{\text{fluid}} + \delta \Psi_{\text{fluid}} = 0$), the Cowling approximation is actually an exact description of the pulsations (Ipser and Lindblom, 1992).

Note that the harmonic spatial dependence expressed in (14) is the signature of the local approach and is valid as long as the wavelength of the perturbations considered is smaller than the length-scale of the radial variations in the equilibrium configuration (this is basically the condition for the WKB approximation) or, stated differently, that

$$k \gg \frac{1}{P} \frac{dP}{d\varpi} \sim \frac{1}{P} \frac{dP}{d\varpi} \sim \frac{1}{L}. \quad (15)$$

Introducing the perturbations (14) in the equilibrium model given by equations (10)–(13) and retaining only the first-order terms, we derive the following perturbation equations (Shu, 1992)

$$i\sigma \delta U + 2\Omega \delta W = ik \delta q, \quad (16)$$

$$(2\Omega + \varpi \partial_\varpi \Omega) i\sigma \delta U + \sigma \delta W = 0, \quad (17)$$

$$i\sigma \delta q - ik c_s^2 \delta U = 0, \quad (18)$$

where $c_s^2 \equiv dP/d\Sigma = \Gamma P/\Sigma$ is the local sound speed. We can now cast equations (16)–(18) into a simple matrix form as

$$\begin{pmatrix} \sigma & 2\Omega & -k \\ \frac{\kappa_r^2}{2\Omega} & \sigma & 0 \\ kc_s^2 & 0 & -\sigma \end{pmatrix} \begin{pmatrix} i\sigma \delta U \\ \delta W \\ i\delta q \end{pmatrix} = 0, \quad (19)$$

where κ_r is the *epicyclic frequency* in the radial direction¹ and is

¹ In principle, an epicyclic oscillation takes places also for motions away

defined as

$$\kappa_r^2 \equiv 2\Omega \left(2\Omega + \varpi \frac{d\Omega}{d\varpi} \right). \quad (20)$$

Note that the radial epicyclic frequency is equal to the orbital frequency for Keplerian orbital motion. i.e. $\kappa_r^2 = \Omega^2$ for $\Omega \sim \varpi^{-3/2}$, and is zero for motions with constant specific angular momentum, i.e. for $\ell \equiv \Omega\varpi^2 = \text{const.}$

Being a homogeneous linear system, a non-trivial solution to the set of equations (19) exists if the determinant of the coefficients matrix is equal to zero, which then provides the dispersion relation

$$\sigma^2 = \kappa_r^2 + k_s^2 c_s^2. \quad (21)$$

This approximate form of the dispersion relation was first applied to waves in accretion discs by Okazaki et al. (1987) and then reconsidered by several authors in more general situations (see Nowak and Wagoner, 1992; Ipser, 1994; Silbergleit et al., 2001). The two terms in the dispersion relation (21) are most easily interpreted when considered separately. To this scope, consider a torus composed of collisionless particles and with specific angular momentum increasing outwards. A fluid element which is infinitesimally displaced from its equilibrium orbit but conserves its angular momentum unchanged, will start oscillating in the radial direction due to a restoring centrifugal force. These oscillations are called *inertial oscillations* and their frequency is the radial epicyclic frequency $\kappa_r(\varpi)$. In compressible fluids, on the other hand, a restoring force due to pressure gradients is also present and is responsible for *acoustic oscillations* with frequency kc_s . Both of these terms contribute to the right-hand-side of the dispersion relation (21) and are collectively referred to as “*inertial-acoustic waves*”. Following a standard convention (Kato, 2001), we will here identify the high frequency modes ($\sigma^2 \gtrsim \kappa_r^2$) with the p modes, or inertial-acoustic modes (Kato and Fukue, 1980) of the vertically integrated torus.

3 RELATIVISTIC TORI: ASSUMPTIONS AND EQUATIONS

As for the Newtonian case, we will here assume that the torus does not contribute to the spacetime metric, which we will take to be that external to a Schwarzschild black hole. This is the simplest, yet non-trivial metric to consider and, more importantly, it allows for a direct comparison with the numerical calculations of Zanotti et al. (2003) (The extension of this work to the Kerr metric will be presented in a future work; Rezzolla and Yoshida, 2003). Furthermore, since we are really interested in the portion of the spacetime in the vicinity of the equatorial plane (i.e. for values of the spherical angular coordinate $|\theta - \pi/2| \ll 1$), we will write the Schwarzschild metric in cylindrical coordinates and retain the zeroth-order terms in the ratio (z/r) (Novikov and Thorne, 1973). In this case, the line element takes the form

$$ds^2 = -e^{2\nu(\varpi)} dt^2 + e^{2\lambda(\varpi)} d\varpi^2 + dz^2 + \varpi^2 d\phi^2, \quad (22)$$

where

$$e^{2\nu(\varpi)} = 1 - \frac{2M}{\varpi} = e^{-2\lambda(\varpi)}. \quad (23)$$

from the background orbital plane. The corresponding frequencies are the vertical epicyclic frequencies but these will not be considered here.

The basic equations to be solved in order to construct equilibrium models are the continuity equation for the rest-mass density ρ

$$\nabla_\alpha(\rho u^\alpha) = 0, \quad (24)$$

and the conservation of energy-momentum

$$\nabla_\alpha T^{\alpha\beta} = 0, \quad (25)$$

where the symbol ∇ refers to a covariant derivative with respect to the metric (22). In equation (25), $T^{\alpha\beta} \equiv (e + p)u^\alpha u^\beta + pg^{\alpha\beta}$ are the components of the stress-energy tensor of a fluid with isotropic pressure p and total energy density e . Since we are dealing with a curved background spacetime, but we want a close comparison with Newtonian expressions, it is useful to introduce an orthonormal tetrad carried by the local static observers and defined by the one-form basis

$$\omega^{\hat{t}} = e^\nu dt, \quad \omega^{\hat{\varpi}} = e^\lambda d\varpi, \quad \omega^{\hat{z}} = dz, \quad \omega^{\hat{\phi}} = \varpi d\phi. \quad (26)$$

In this frame, the components of the fluid four-velocity are denoted by $u^{\hat{\mu}}$ (with $\mu = t, \varpi, z, \phi$), and the 3-velocity components are then given by

$$v^{\hat{i}} = \frac{u^{\hat{i}}}{u^{\hat{t}}} = \frac{\omega^{\hat{i}} u^\alpha}{\omega^{\hat{t}} u^\alpha}, \quad i = \varpi, z, \phi. \quad (27)$$

In analogy with the Newtonian case presented in Section 2, we use the vertically integrated quantities defined in (1)–(2) and assume that they obey an effective polytropic equation of state of the type (4). Enforcing the conditions of hydrostatic equilibrium and of axisymmetry simplifies the hydrodynamical equations considerably, reducing them to Bernoulli-type equations (Kozłowski et al., 1978)

$$\frac{\nabla_i p}{e + p} = -\nabla_i \ln(u_t) + \frac{\Omega \nabla_i \ell}{1 - \Omega \ell}, \quad (28)$$

where $\ell \equiv -u_\phi/u_t$ is the specific angular momentum (i.e. the angular momentum per unit energy). Simple algebraic manipulations show that the only relevant component of equations (28), i.e. the radial one, can be written explicitly as

$$\frac{\partial_\varpi p}{e + p} = -\frac{e^{2\nu} \partial_\varpi \nu - \Omega^2 \varpi}{e^{2\nu} - \Omega^2 \varpi^2}. \quad (29)$$

which represents a generic condition for the existence of hydrostatic equilibrium of a fluid configuration orbiting around a Schwarzschild black hole. Note also that a number of cancellations have removed any dependence on the spatial derivative of the angular velocity from the right-hand-side of equation (29).

Being interested in vertically integrated expressions, we need to integrate both sides of equation (29). Interestingly, in the spacetime (22) the right-hand-side of (29) is a function of the cylindrical radial coordinate only, and hence its vertical integration simply yields a new multiplicative factor $2H$. The left-hand-side, on the other hand, cannot be managed unless a simplifying assumption is made and this amounts to consider that the total enthalpy $(e + p)$ is only a weak function of the z -coordinate so that, effectively, it is possible to substitute it with its vertically averaged value $(\bar{e} + \bar{p})$, where

$$e(\varpi, z) + p(\varpi, z) \approx \bar{e}(\varpi) + \bar{p}(\varpi) \equiv \frac{1}{2H} \int_{-H}^H (e + p) dz. \quad (30)$$

With this assumption, the vertically integrated equation (29) can be written as

$$\frac{1}{E + P} \frac{dP}{d\varpi} = -\frac{\varpi}{\varpi - 2M - \Omega^2 \varpi^3} \left(\frac{M}{\varpi^2} - \Omega^2 \varpi \right), \quad (31)$$

where E is the vertically integrated energy density

$$E \equiv \int_{-H}^H e dz = \frac{P}{\Gamma - 1} + \Sigma \approx \frac{P}{\gamma - 1} + \Sigma. \quad (32)$$

We next introduce perturbations in the velocity and pressure with a harmonic time dependence of the type

$$\begin{pmatrix} \delta V^{\hat{\omega}} \\ \delta V^{\hat{\phi}} \\ \delta Q \end{pmatrix} \sim e^{-i\sigma t}, \quad (33)$$

where $\delta Q \equiv \delta P/(E+P)$, and where we have defined the averaged velocity perturbations as

$$\delta V^{\hat{\omega}} \equiv \frac{1}{2H} \int_{-H}^H \delta v^{\hat{\omega}} dz, \quad \delta V^{\hat{\phi}} \equiv \frac{1}{2H} \int_{-H}^H \delta v^{\hat{\phi}} dz. \quad (34)$$

After perturbing the hydrodynamical equations (24)–(25) and taking the vertically integration of the resulting equations, we derive the following set of equations

$$i\sigma e^{\nu-\lambda} \delta V^{\hat{\omega}} + 2e^{\nu-2\lambda} \Omega \left(1 + \frac{\varpi}{E+P} \frac{dP}{d\varpi} \right) \delta V^{\hat{\phi}} + A e^{-2\lambda} \frac{d(\delta Q)}{d\varpi} = 0, \quad (35)$$

$$i\sigma \delta V^{\hat{\phi}} - \left(\frac{d\Omega}{d\varpi} + \frac{2}{\varpi} \Omega - 2\Omega \frac{d\nu}{d\varpi} \right) \varpi e^{-\lambda} \delta V^{\hat{\omega}} + i\sigma A \Omega e^{-2\nu} \varpi \delta Q = 0, \quad (36)$$

$$i\sigma \left(\frac{E+P}{\Gamma P} \right) \delta Q - e^{\nu-\lambda} \frac{d(\delta V^{\hat{\omega}})}{d\varpi} - i\sigma \frac{\varpi e^{\nu}}{A} \Omega \delta V^{\hat{\phi}} - \left[2 \frac{d\nu}{d\varpi} + \frac{1}{\varpi} - \frac{1}{2A} \frac{dA}{d\varpi} + \frac{1}{\Gamma P} \frac{dP}{d\varpi} \right] e^{\nu-\lambda} \delta V^{\hat{\omega}} = 0, \quad (37)$$

where $A \equiv 1/(u_t)^2$. Equations (35)–(37) represent the ϖ and ϕ -components of the perturbed relativistic Euler equations as well as the perturbed continuity equation.

4 PERTURBATIONS OF RELATIVISTIC TORI: A LOCAL ANALYSIS

A local analysis of the perturbed hydrodynamical equations (35)–(37) can be performed after introducing a harmonic radial dependence of the type $\delta Q, \delta V^{\hat{\omega}}, \delta V^{\hat{\phi}} \sim \exp(ik\varpi)$, where k is the radial wavenumber and, again, we will assume that $\lambda = 2\pi/k \ll L$. Simple considerations allow now to remove some of the terms in the continuity equation (37), thus simplifying it further. In particular, it is easy to realize that the third and fourth terms in equation (37) are very small as compared to the first and second ones, to which they are similar in nature. More specifically, both the second and the fourth terms involve the radial velocity perturbation but with coefficients proportional to k and $1/L$, respectively. Assuming that the condition (14) is satisfied, it is then reasonable to drop the fourth term of equation (37). Similarly, the ratio between the third and the first term can be approximated as

$$\frac{\delta V^{\hat{\phi}}}{\delta Q} \frac{\Gamma P \varpi \Omega e^{\nu}}{(E+P)A} \sim \mathcal{O} \left(\frac{\delta V^{\hat{\phi}}}{\delta Q} \right) \times \mathcal{O}(|\text{typical velocity}|^3), \quad (38)$$

where we have approximated the first term as $\sim \delta P/(\Gamma P) \sim \delta Q/c_s^2$ and the third one as $\sim (\varpi \Omega) \delta V^{\hat{\phi}}$. While $(\delta V^{\hat{\phi}}/\delta Q)$ is the ratio of two perturbed quantities and of order unity, the typical velocity of is of the order of the orbital velocity at the marginally stable circular orbit (i.e. $\sim 1/\sqrt{6}$) so that, overall, the ratio in (38) is much smaller than unity and the third term in equation (37) can therefore also be dropped. Finally, it should be noted that the third term on the left hand side of equation (36) can also be discarded, as it would introduce a purely imaginary part in the dispersion relation (42). This term, which is due a time derivative of the pressure in the Euler equations, has a purely relativistic origin and has been found to provide negligible contributions in the numerical solution of the system (35)–(37).

We can now introduce quantities that are more directly related to the ones used in the Newtonian example of Section 2, namely

$$\delta U \equiv i\delta V^{\hat{\omega}}, \quad \delta W \equiv \delta V^{\hat{\phi}}, \quad (39)$$

so that the linearized perturbation equations in the unknowns δU , δW and δQ can be written as a homogeneous linear system

$$\mathcal{M}(k, \sigma) \begin{pmatrix} \delta U \\ \delta W \\ \delta Q \end{pmatrix} = 0, \quad (40)$$

where the matrix of coefficients \mathcal{M} depends both on k and σ . Imposing the determinant of \mathcal{M} to be zero, we obtain the dispersion relation

$$\sigma^3 - \sigma e^{-2\lambda} \left[2\Omega \left(2\Omega + \varpi \frac{d\Omega}{d\varpi} - 2\varpi \Omega \frac{d\nu}{d\varpi} \right) \left(1 + \frac{\varpi}{E+P} \frac{dP}{d\varpi} \right) + e^{2\nu} (1 - e^{-2\nu} \varpi^2 \Omega^2) k^2 \frac{\Gamma P}{E+P} \right] = 0. \quad (41)$$

A non-trivial solution of (41) is given by

$$\sigma^2 = \kappa_r^2 + [e^{2(\nu-\lambda)} (1 - e^{-2\nu} \varpi^2 \Omega^2)] k^2 c_s^2, \quad (42)$$

where now $c_s^2 \equiv dP/dE$ is the square of the relativistic sound velocity in the vertically integrated disc. The dispersion relation (42) represents the relativistic generalization of (21) in which we have defined the relativistic radial epicyclic frequency for an extended fluid object κ_r as

$$\kappa_r^2 \equiv 2e^{-2\lambda} \Omega \left(2\Omega + \varpi \frac{d\Omega}{d\varpi} - 2\varpi \Omega \frac{d\nu}{d\varpi} \right) \left(1 + \frac{\varpi}{E+P} \frac{dP}{d\varpi} \right). \quad (43)$$

A number of comments should now be made about this expression. Firstly, while the definition (43) reduces to the corresponding expression (20) when the Newtonian limit is taken, it has a new important correction coming from pressure gradients (cf. second term in the second round brackets, which is a function of ϖ only). Secondly, in those cases in which the (radial) pressure gradients can be neglected (e.g. for very thin discs), the fluid motion is essentially Keplerian and expression (43) coincides with the relativistic radial epicyclic frequency for a point-like particle. In this case, and only in this case, (43) reduces to the expression for the radial epicyclic frequency derived by Okazaki et al. (1987) that, for a Schwarzschild spacetime in spherical coordinates, is

$$(\kappa_r)_{\text{Keplerian}} = \sqrt{\left(1 - \frac{6M}{r} \right) \frac{GM}{r^3}}. \quad (44)$$

Model	ℓ -distribution	$\tilde{\ell}_c$	α, β	q	$\tilde{\omega}_{\text{in}}$	$\tilde{\omega}_{\text{out}}$	$\tilde{\omega}_{\text{cusp}}$	$\tilde{\omega}_{\text{max}}$	ΔW_{in}
(c1)	const.	3.90	—	—	4.241	36.26	4.233	9.457	-1.0×10^{-6}
(c2)	const.	3.75	—	—	4.882	11.57	4.836	7.720	-1.0×10^{-5}
(c3)	const.	3.70	—	—	5.538	8.227	5.266	6.921	-1.0×10^{-4}
(l1)	linear	—	0.03, 3.70	—	5.115	46.71	4.444	10.13	-1.0×10^{-4}
(l2)	linear	—	0.01, 3.70	—	5.224	12.74	4.845	8.087	-1.0×10^{-5}
(pl1)	power-law	3.70	—	0.02	4.872	20.97	4.520	9.108	-1.0×10^{-5}
(pl2)	power-law	3.60	—	0.05	5.065	61.98	4.312	11.06	-1.0×10^{-5}
(pl3)	power-law	3.66	—	0.02	5.157	15.46	4.694	8.596	-1.0×10^{-5}
(pl4)	power-law	3.68	—	0.03	4.854	32.13	4.395	9.889	-1.0×10^{-6}

Table 1. Main properties of the two non constant angular momentum models considered. From left to right the columns report: the type of angular momentum distribution (see Section 7 for a description of $\tilde{\ell}_c$, α , β and q), the inner and the outer radii of the torus $\tilde{\omega}_{\text{in}}$ and $\tilde{\omega}_{\text{out}}$, the radial position of the maximum density in the torus $\tilde{\omega}_{\text{max}}$, and the value of the potential gap chosen at the inner edge of the torus.

An important feature of the relativistic radial epicyclic frequency (44), and that distinguishes it from the corresponding expression (43), is that such a function is not monotone in ϖ but has a maximum at a given radius, thus indicating that in General Relativity oscillation modes can be trapped near the inner edge of an accretion disc (Kato and Fukue, 1980). When pressure gradients are taken into account, however, this ceases to be true and the epicyclic frequency becomes monotonically decreasing with radius (cf. Figure 5)

Finally, it should be noted that, as for the Newtonian case, expression (43) predicts a *zero epicyclic frequency for orbital motion with constant specific angular momentum*. Note that this holds true only when the specific angular momentum is defined as $\ell \equiv -u_\phi/u_t$, in which case

$$\frac{d\ell}{d\varpi} = \frac{d}{d\varpi}(\varpi^2 e^{-2\nu} \Omega) = \varpi e^{-2\nu} \left(2\Omega + \varpi \frac{d\Omega}{d\varpi} - 2\varpi \Omega \frac{d\nu}{d\varpi} \right). \quad (45)$$

To the best of our knowledge, this result has not been discussed before in the literature for finite-size fluid configurations. Furthermore, it is relevant for the physical interpretation of the modes found in the numerical calculations of Zanotti et al. (2003) as it indicates that the oscillations found in those simulations cannot be associated (at least within the validity of a vertically integrated approach) with epicyclic oscillations, but should be associated with other restoring forces, most notably pressure gradients.

5 PERTURBATIONS OF RELATIVISTIC TORI: A GLOBAL ANALYSIS

A global analysis of the axisymmetric oscillations modes of a relativistic torus consists of solving the system of equations (35)–(37) as an eigenvalue problem, treating the perturbed quantities as eigenfunctions and the unknown σ as the eigenfrequency (see Rodriguez et al., 2002 for the solution of the equivalent problem for relativistic thin discs).

It is worth remarking that equation (28) basically states that a condition for the existence of stationary, geometrically thick fluid configurations orbiting around a Schwarzschild black hole is that the distribution of angular momentum is a non-Keplerian one. As long as this condition is met, in fact, the left-hand-side of equation (28) will not be zero and the pressure gradients will expand the disc in the vertical direction. Of course, different distributions of

angular momentum will define tori with different properties such as: different inner and outer radii, different positions for the maximum in density, etc. Among the infinite number of possible angular momentum distributions, those that produce tori with a finite radial extension are of particular interest, since they allow for the existence of globally trapped, axisymmetric modes of oscillation.

Because of the degeneracy in the functional form for $\ell(\varpi)$, we have constructed several different models that we have reported in Table 1 and that we will be discussing in detail in the following Sections. This approach to the problem is clearly more expensive as the eigenvalue problem needs to be solved for a large number of models; however it also allows one to investigate how the axisymmetric oscillations depend on the angular momentum distribution. When features are found which do not depend on a specific choice for the distribution of angular momentum and that are thus indication of a universal behaviour, this approach can be very rewarding as we will discuss in the following Sections.

However, before discussing the results of the numerical solution of the eigenvalue problems, it is useful to review briefly the numerical approach followed in the solution of the eigenvalue problem and the boundary conditions imposed.

5.1 Numerical method

Equations (35)–(37), supplemented with suitable boundary conditions at both edges of the numerical grid, represent a standard two-point boundary value problem, for which a “shooting” method can be used. In practice, given a trial value for the eigenfrequency σ , two solutions for the unknown quantity (either δQ or δU) are found starting from the two edges of the numerical grid at the inner, ϖ_{in} , and outer, ϖ_{out} , radii of the torus. These two solutions are then matched at an arbitrary point ϖ_{M} in the domain, where the Wronskian of the left and right solutions is evaluated. This procedure is iterated until a zero of the Wronskian is found with the desired accuracy, thus determining both the eigenfrequency and the eigenfunctions of the mode considered.

Note that because of the linearity of the present analysis, the solutions are invariant after a rescaling of all the quantities by a constant. In practice, this freedom allows to choose the initial guess for one of the eigenfunctions at one edge of the numerical grid to be a freely specifiable number, which we typically set to one. Furthermore, since the spacetime is uniquely described once the mass M of the black hole has been fixed, we can use it to rescale

all of the relevant quantities involved in the calculations. The new dimensionless quantities, indicated with a “tilde”, are then defined as

$$\varpi \equiv \tilde{\varpi} \left(\frac{M}{M_\odot} \right) \left(\frac{GM_\odot}{c^2} \right), \quad (46)$$

$$\Sigma \equiv \tilde{\Sigma} \left(\frac{M}{M_\odot} \right)^{-1} \left(\frac{GM_\odot}{c^2} \right)^{-2} M_\odot, \quad (47)$$

$$P \equiv \tilde{P} \left(\frac{M}{M_\odot} \right)^{-1} \left(\frac{GM_\odot}{c^2} \right)^{-2} M_\odot c^2, \quad (48)$$

$$K \equiv \tilde{K} \left(\frac{M}{M_\odot} \right)^{\Gamma-1} \left(\frac{GM_\odot}{c^2} \right)^{2(\Gamma-1)} (M_\odot)^{1-\Gamma} c^2, \quad (49)$$

$$\sigma \equiv \tilde{\sigma} \left(\frac{M}{M_\odot} \right)^{-1} \left(\frac{GM_\odot}{c^2} \right)^{-1} c, \quad (50)$$

$$\ell \equiv \tilde{\ell} \left(\frac{M}{M_\odot} \right) \left(\frac{GM_\odot}{c^2} \right) c. \quad (51)$$

Unless specified differently, all of the results presented hereafter will be given in terms of these dimensionless quantities.

5.2 Boundary conditions

Suitable boundary conditions need to be specified at the inner and outer edges of the vertically integrated torus for the solution of the set of equations (35)–(37). As for oscillations in stars, we here assume the perturbed surface of the torus to be where the Lagrangian pressure perturbation vanishes, i.e. where

$$\Delta p = 0. \quad (52)$$

Because the Eulerian and Lagrangian descriptions are linked through the relation

$$\Delta = \delta + \mathcal{L}_{\vec{\xi}}, \quad (53)$$

where $\mathcal{L}_{\vec{\xi}}$ is the Lie derivative along the Lagrangian displacement three-vector $\vec{\xi}$, condition (52) can also be written as

$$\delta p + \xi^j \partial_j p = 0, \quad (54)$$

from which it follows that $\Delta p = 0 = \delta p$ for a polytropic fluid configuration whose rest-mass density vanishes at the surface (Tassoul, 1978). Note also that while in the Cowling approximation the Eulerian perturbation of the metric, δg_{ab} is zero, the Lagrangian perturbation $\Delta g_{ab} = \delta g_{ab} + \mathcal{L}_{\vec{\xi}} g_{ab} = \nabla_a \xi_b + \nabla_b \xi_a$ is, in general, nonzero.

Using the relation between the perturbed 4-velocity u^α and the Lagrangian perturbation of the metric (see Friedman 1978),

$$\Delta u^\alpha = \frac{1}{2} u^\alpha u^\beta u^\gamma \Delta g_{\beta\gamma}, \quad (55)$$

which, in our case, reduces to the relation,

$$\xi^\varpi = \frac{i e^{\nu-\lambda} \delta V^{\hat{\varpi}}}{\sigma}, \quad (56)$$

we can write the boundary condition (52) simply as

$$\delta Q + \frac{e^{\nu-\lambda}}{\sigma(E+P)} \frac{dP}{d\varpi} \delta U = 0. \quad (57)$$

Expression (57), taken as a linear relation between δQ and δU , provides us with the boundary conditions to be imposed at the inner and outer edges of the torus.

6 CONSTANT SPECIFIC ANGULAR MOMENTUM TORI

The simplest and most studied choice for the distribution of angular momentum is the one in which $\ell = \ell_c = \text{const.}$, with ℓ_c being chosen in the interval between the specific angular momentum at the marginally stable orbit $\ell_{\text{ms}} = 3\sqrt{6}/2 \simeq 3.67$ and the one at the marginally bound orbit $\ell_{\text{mb}} = 4$, to yield a disc of finite size. Besides yielding a simpler approach, constant specific angular momentum tori benefit from having a radial epicyclic frequency which is identically zero [cf. eqs. (43) and (45)], thus leaving pressure gradients as the only possible restoring forces. As a result, a constant angular momentum distribution provides an interesting limit for the properties of p -mode oscillations that will not be influenced by centrifugal effects.

The procedure for the construction of the background model for the torus can be summarized as follows. Firstly, after a value ℓ_c for the constant specific angular momentum has been chosen, the locations of the cusp ϖ_{cusp} and of the maximum density in the torus² ϖ_{max} are determined as the positions at which the Keplerian specific angular momentum is equal to ℓ_c . The inner and outer edges of the torus can then be calculated after requiring that they lie on the same equipotential surface, i.e.

$$u_t(\varpi_{\text{in}}) = u_t(\varpi_{\text{cusp}}) \exp(\Delta W_{\text{in}}) = u_t(\varpi_{\text{out}}), \quad (58)$$

where ΔW_{in} is the value of the potential gap chosen at the inner edge of the torus and is therefore a measure of how much the torus “fills” its Roche lobe. Clearly, the case in which $\Delta W_{\text{in}} = 0$ corresponds to a torus filling its outermost closed equipotential surface (i.e. the one possessing a cusp)

Having determined ϖ_{in} , it is then possible to calculate the angular velocity distribution as

$$\Omega = \Omega_c \left(\frac{\varpi - 2M}{\varpi_c - 2M} \right) \left(\frac{\varpi_c}{\varpi} \right)^3, \quad (59)$$

where Ω_c is angular velocity at the radial position of cusp ϖ_{cusp} . Finally, after making a choice for the parameters of the equation of state (and therefore for k and γ) the equation for the hydrostatic equilibrium (31) can be integrated, either numerically or analytically (Kozłowski et al., 1978), to build the torus model which will serve as background for the introduction of the perturbations.

When the specific angular momentum is constant within the torus, also the perturbation equations become simpler and, in particular, the second term in (36) vanishes exactly [cf. equation (45)] and the resulting set of equations can then be written as

$$\sigma \delta U + A e^{-\nu-\lambda} \frac{d(\delta Q)}{d\varpi} = 0, \quad (60)$$

$$\delta V^{\hat{\phi}} + A \Omega e^{-2\nu} \varpi \delta Q = 0, \quad (61)$$

$$\begin{aligned} \sigma \delta Q + e^{\nu-\lambda} \frac{\Gamma P}{E+P} \frac{d(\delta U)}{d\varpi} + \frac{e^{\nu-\lambda} \Gamma P}{E+P} \times \\ \times \left[2 \frac{d\nu}{d\varpi} + \frac{1}{\varpi} - \frac{1}{A} \frac{dA}{d\varpi} + \frac{1}{\Gamma P} \frac{dP}{d\varpi} \right] \delta U = 0. \end{aligned} \quad (62)$$

Equations (60)–(62) have been solved numerically for a number of different models, whose main properties, such as the inner

² Note that the position of the maximum density in the torus is traditionally referred to as the “centre” of the torus, although its coordinate centre is, of course, at $\varpi = z = 0$.

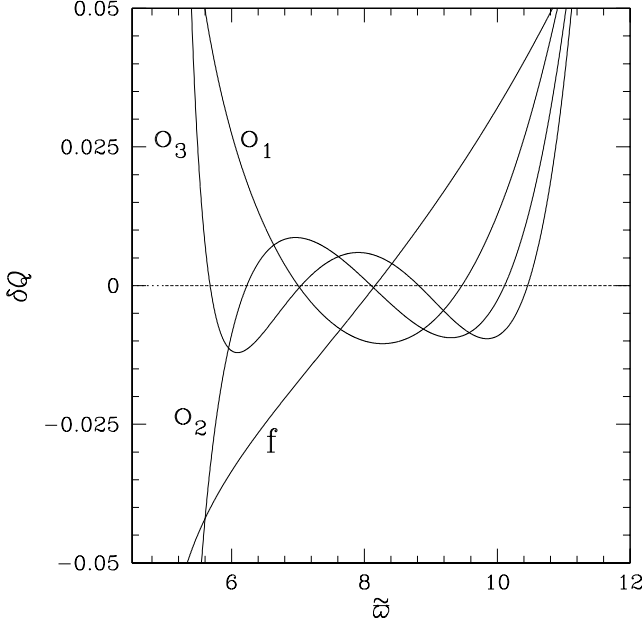


Figure 1. Eigenfunctions for $\delta Q = \delta P/(E + P)$ as a function of the radial coordinate for a constant angular momentum disc. Only the fundamental mode f and the first three overtones, denoted by o_1 , o_2 and o_3 , have been reported. The data refers to model (c2) of Table 1 and the units on the vertical axis are arbitrary.

and outer radii $\tilde{\omega}_{\text{in}}$, $\tilde{\omega}_{\text{out}}$, the position of the maximum in the surface density distribution $\tilde{\omega}_{\text{max}}$, and the value of the specific angular momentum at the inner edge of the disc $\ell_c \equiv \ell(\tilde{\omega}_{\text{in}})$, are summarized in Table 1. As a representative example, we present in Figures 1 and 2 the results for a torus model with $\ell_c = 3.75$ [i.e. model (c2) of Table 1].

Figure 1, in particular, shows the solution for the eigenfunction δQ for both the fundamental mode f and for the first three overtones o_1 , o_2 and o_3 . Similarly, Figure 2 shows the fundamental mode and the first three overtones for the eigenfunction δU , which has always one node less than δQ . Note that the choice of a very small potential barrier introduces complications in the numerical solution of the eigenvalue problem. For a model with $\Delta W_{\text{in}} = 0$, in fact, the fluid elements at the inner edge are just marginally stable to accretion onto the black hole. This behaviour is reflected in the eigenfunctions δQ and δU , which tend to diverge at the inner and outer edges of the torus. To avoid this problem (still partially visible in Figures 1 and 2) we have used a small but nonzero value, $\Delta W_{\text{in}} = -10^{-5}$, for the potential barrier.

A careful look at Figures 1 and 2 reveals that the modes f and o_2 have similar properties at the inner edge; furthermore, during each half-period, they have signs which are opposite to those of the modes o_1 and o_3 . This is an important feature indicating that not all modes will behave in the same manner at the inner edge where mass-loss and accretion onto the black hole take place. While a conclusion on this behaviour cannot be drawn on the basis of the present linear analysis, in which the total mass is conserved exactly ($\Sigma \delta U = 0$ at the inner and outer edges for all modes), the functional form of the eigenfunctions for δQ and δU seems to suggest that mass accretion through the cusp will be possible preferably at the frequencies corresponding to the f , and o_{2n} modes (see also the

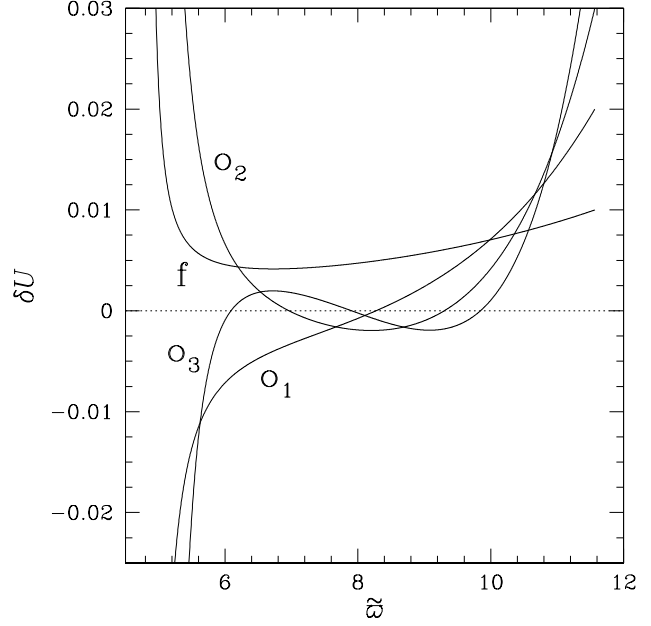


Figure 2. Eigenfunctions for $\delta U = i\delta V^{\tilde{\omega}}$ as a function of the radial coordinate for a constant angular momentum disc. Only the fundamental mode f and the first three overtones, denoted by o_1 , o_2 and o_3 , have been reported. The data refers to model (c2) of Table 1 and the units on the vertical axis are arbitrary.

discussion below for a comparison with the numerical calculations presented in Zanotti et al., 2003).

The eigenfrequencies corresponding to model (c2), as well as for all of the other models in Table 1, are listed in Table 2, where we have included the frequencies up to the fourth overtone. A careful look at Table 2 reveals that the computed eigenfrequencies are, at least for the first few modes, in a sequence 2:3:4:..., to a good precision. As the order of the mode increases, this simple sequence is no longer followed and a different one appears. The fact that the lowest order modes appear at frequencies that are in small integer ratios is not particularly surprising if p modes are to be interpreted as sound waves trapped within the cavity represented by the confined torus. In this case, in fact, one would indeed expect that modes should be trapped and with wavelengths that are multiples of the trapping lengthscale, i.e. $\lambda_n = [2/(2+n)]L$, where $n = 0, 1, \dots$. Stated differently, the results reported in Table 2 are consistent with the idea that p modes can be associated with sound waves trapped in the torus and having frequencies which are multiples of the fundamental one and given by $\sigma_n = c_s/\lambda_n = [(2+n)/2]f$.

Note that while these p modes follow the same definition and are similar in nature to the ones discussed by Nowak and Wagoner (1991, 1992) for thin discs, their trapping is not produced by a turning of the relativistic radial epicyclic frequency at smaller radii. Rather, the relativistic radial epicyclic frequency in discs in which pressure gradients play an important role, has been found to be monotonically decreasing for all of the disc models considered here [cf. equation (43), Fig. 5]. An important consequence of this is that the p modes for thick discs are *not restricted* to be trapped in special parts of the disc, as it happens for the corresponding p modes for thin discs (Nowak & Wagoner 1991, 1992). In particular, they need to be present only in the (rather small) inner regions of the disc, where they can produce only a slight modulation in the

Model	f	o_1	o_2	o_3	o_4
(c1)	0.00838	0.01227	0.01604	0.01973	0.02337
(c2)	0.02017	0.02950	0.03700	0.04322	0.04869
(c3)	0.01898	0.02764	0.03514	0.04230	0.04933
(l1)	0.00602	0.00831	0.01060	0.01287	0.01514
(l2)	0.01992	0.02856	0.03618	0.04330	0.05019
(pl1)	0.01447	0.02114	0.02733	0.03324	0.03894
(pl2)	0.00426	0.00616	0.00803	0.00988	0.01172
(pl3)	0.01810	0.02635	0.03764	0.04073	0.04742
(pl4)	0.00948	0.01379	0.01792	0.02196	0.02593

Table 2. Eigenfrequencies of the fundamental f mode and of the first four overtones o_n of the vertically integrated models described in Table 1. All the frequencies are given in normalized units.

disc emission. Similarly, they are not constrained to be trapped the outer regions of the disc, where the location of the outer radius remains uncertain and the corresponding frequencies very small. On the contrary, the modes discussed here are present over the whole torus, which then behaves as a *single* trapping cavity. This is a substantial difference, giving these modes the possibility of possessing frequencies comparable with observations and of causing non-negligible modulations in the disc emission.

Having solved the eigenvalue problem for p modes in vertically integrated relativistic tori with constant specific angular momentum, we can now proceed to a comparison with the fully nonlinear two-dimensional simulations discussed by Zanotti et al. (2003). This is presented in Figure 3 where we have plotted the power spectra of the L_2 norms of the rest-mass density for the torus model (c2) in Table 1. The solid line, in particular, refers to initial data in which a global perturbation has been introduced in terms of the radial velocity field of a relativistic spherical accretion solution [cf. equation (15) of Zanotti et al., 2003]. Clearly, the power spectrum for the continuous line shows the presence of peaks appearing in a simple small integer sequence 2:3:4:..., providing convincing evidence that the oscillations triggered in the simulations of Zanotti et al. (2003) correspond indeed to p -modes oscillations of perturbed relativistic tori. It should also be noted that this sequence is not the same shown by the peaks in the power spectrum of the mass accretion rate onto the black hole, which instead are only in the sequence 1:2:3:... (cf. Figure 7 of Zanotti et al., 2003). This difference remains puzzling, but could be explained on the basis of the behaviour of the eigenfunctions for the f and o_{2n} modes at the inner edge discussed above. In this case, in fact, all of the o_{2n+1} modes would have vanishingly small perturbations at the inner edge of the disc and would not produce a mass accretion at those frequencies, as shown by Figure 7 of Zanotti et al. (2003).

The knowledge of the eigenfunctions of p modes in relativistic tori can also be used to go a step beyond a simple comparison with numerical simulations and actually use the latter to perform investigations of “numerical” discoseismology. In other words, having a complete picture of the oscillation properties and an accurate two-dimensional numerical code to simulate them, it is possible to investigate the dynamical response of a relativistic thick disc as a result of the introduction of suitably selected perturbations. As a concrete example, we report with the dashed line in Figure 3 the power spectrum of the L_2 norm of the rest-mass density for the torus model (c2) in Table 1. The important difference with the corresponding spectrum indicated with a solid line is that the dashed

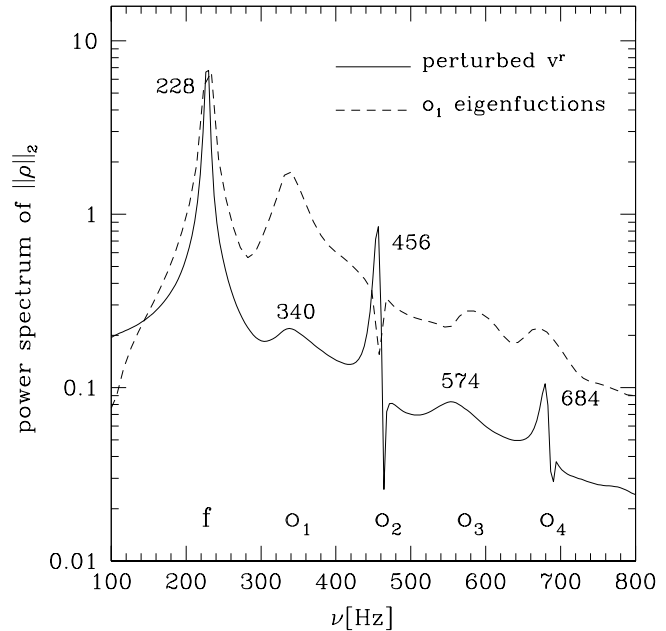


Figure 3. Power spectra of the L_2 norm of the rest-mass density for the torus model (c2) in the Table 1 of Zanotti et al. (2003). Different lines refer to models with different initial perturbations. The solid line, in particular, refers to initial data in which a global perturbation has been introduced in the radial velocity field only [cf. equation (15) of Zanotti et al. (2003)]. The dotted line, on the other hand, refers to initial data in which a perturbation based on the computed eigenfunctions of the o_1 mode has been introduced both in the radial velocity and in the density. The two spectra have been rescaled in order to match in the power of the fundamental frequency.

line refers to a simulation having as initial data perturbations based on the computed eigenfunctions for δU and δQ of the o_1 mode. This represents a selective excitation of the o_1 mode and, as a result, the corresponding power in the first overtone is increased by almost a factor of ten (the power in the o_2 mode is instead decreased of a similar amount). This behaviour further confirms that the p modes derived in this perturbative analysis correspond to the modes simulated numerically by Zanotti et al. (2003). Finally, it should be noted that the power spectrum corresponding to initial data containing only an o_1 -mode perturbation shows that also the other modes have been excited, most notably the fundamental one. This is due partly to a mode-mode coupling which transfers energy from one mode to the other ones, but also to the error introduced using eigenfunctions derived for a vertically integrated model, and that cannot reproduce the corresponding eigenfunctions of a two-dimensional disc exactly.

There is a final aspect of the axisymmetric p modes discussed so far which is worth underlining. This is illustrated in Figure 4 where we have plotted the values of the eigenfrequencies for the fundamental mode f (solid line) and for the first overtone o_1 (dashed line) for large number of tori. All of the points on the solid and dashed curves in Figure 4 represent the solution of the eigenvalue problem and the two sequences have been calculated for tori with fixed “centre” $\tilde{\omega}_{\max} = 10.17$, but having different radial extensions $\tilde{L} \equiv \tilde{\omega}_{\text{out}} - \tilde{\omega}_{\text{in}}$. As one would expect for modes behaving effectively as sound waves, the eigenfrequencies decrease as the radial extent of the torus increases. Furthermore, the frequencies for f and o_1 maintain a harmonic ratio 2:3 for all the values of \tilde{L} . Most importantly, however, the filled dot shown in Figure 4 for $\tilde{L} = 0$

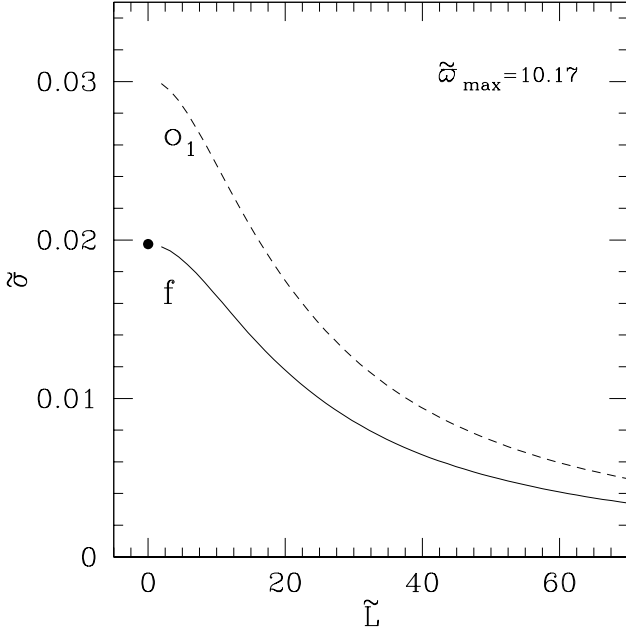


Figure 4. Eigenfrequencies for the fundamental f (solid line) and for the first overtone o_1 (dashed line) of axisymmetric p modes for $\ell = \text{const.}$ tori. The two lines refer to sequences of tori having the same radial position for the “centre” $\tilde{\omega}_{\text{max}} = 10.17$, but different radial extensions $\tilde{L} \equiv \tilde{\omega}_{\text{out}} - \tilde{\omega}_{\text{in}}$. The filled dot represents the radial epicyclic frequency for a circular orbit at $\tilde{\omega}_{\text{max}}$ and thus the value at which the fundamental p -mode frequency tends in the limit of a vanishing torus size.

represents the radial epicyclic frequency for a circular orbit at $\tilde{\omega}_c$, i.e. $\tilde{\sigma} = \sqrt{(1 - 6/\tilde{\omega}_c)GM/\tilde{\omega}_c^3}$.

This is an important result that provides a simple interpretation of the nature of the axisymmetric p modes of thick discs: *the radial epicyclic frequency at the position of maximum density represents the value at which the fundamental p -mode frequency tends in the limit of a vanishing torus size.* The importance of this result is that while different models for the tori, using, for instance, different equations of state or different angular momentum distributions, will produce different slopes for the solid and dashed lines in Figure 4, all of the sequences will terminate on the filled dot when $L \rightarrow 0$, that is, when finite-size effects will cease to be relevant and each torus will effectively behave as a ring of particle in circular orbits. Because this occurs only in the limit $L \rightarrow 0$, it should not surprise that it is valid also for sequences of tori with constant distributions of specific angular momentum for which, as discussed in Section 4, the epicyclic frequency is zero. Indeed, this result is totally independent of the distribution of specific angular momentum and will be confirmed in the following Section, where tori with non-constant specific angular momentum distributions are considered. An analytic proof of this conclusion is provided in Appendix A.

7 NON-CONSTANT SPECIFIC ANGULAR MOMENTUM TORI

While the study of constant angular momentum discs offers several advantages and simplifies the equations, realistic disc are likely to have angular momentum distributions that are not constant. For this reason, and in order to assess the validity of the results derived so

far with more generic distributions of angular momentum, we have extended our mode analysis also to discs with non-constant angular momentum. The first step in this direction consists of determining which distribution of specific angular momentum $\ell = \ell(\varpi)$ should be specified in the construction of an equilibrium model. This choice is, to some extent, arbitrary with the only constraint being given by *Rayleigh’s criterion* for the dynamical stability against axisymmetric perturbations (Tassoul 1978). This condition, however, is not very strong and simply requires that $d\ell/d\varpi \geq 0$, so that even a constant angular momentum distribution is stable, although only marginally.

Some guidance in this choice can come from numerical simulations and indeed calculations of torus formation performed by Davies et al. (1994) with smooth particle hydrodynamics (SPH) techniques have shown that the final configuration consists of a core object surrounded by a torus whose angular momentum distribution is close to a power-law in radius, with index 0.2. In our computations we have therefore adopted two simple and different distributions for the specific angular momentum that can be expressed analytically. We refer to the first one as the “linear” distribution, in which

$$\ell = \alpha\varpi + \beta, \quad (63)$$

where α and β are adjustable constant coefficients. Similarly, we refer to the second one as the “power-law” distribution, in which instead

$$\ell = \ell_c \varpi^q, \quad (64)$$

where q is also an arbitrary parameter. The values chosen for α , β , ℓ_c and q for the representative models discussed here have been summarized in Table 1. Note that we have deliberately chosen small values for both α and q and this is to avoid the construction of unperturbed models that differ significantly in radial extension from the ones built with a constant specific angular momentum distribution³.

The construction of the equilibrium models proceeds in this case as discussed in the previous Section, namely, by first fixing an initial value for the specific angular momentum at the cusp, then by calculating the radial extension of the torus in terms of the potential barrier ΔW_{in} , and finally by integrating numerically equation (29) for the chosen distribution of $\Omega(\varpi)$.

The full system of the perturbed equations (35)–(37), can now be rewritten in a more compact form as

$$0 = \sigma\delta Q + e^{\nu-\lambda} \frac{\Gamma P}{E+P} \frac{d(\delta U)}{d\varpi} + \frac{e^{\nu-\lambda} \Gamma P}{E+P} \left[2 \frac{d\nu}{d\varpi} + \frac{1}{\varpi} - \frac{1}{A} \frac{dA}{d\varpi} + \frac{1}{\Gamma P} \frac{dP}{d\varpi} \right] \delta U - \sigma \frac{e^{\nu} \Omega}{A} \left(\frac{\varpi}{E+P} \right) \frac{dP}{d\varpi}, \quad (65)$$

$$0 = \sigma\delta U + A e^{-\nu-\lambda} \frac{d(\delta Q)}{d\varpi} + 2e^{-\lambda} \Omega \left(1 + \frac{\varpi}{E+P} \frac{dP}{d\varpi} \right) \delta W, \quad (66)$$

$$0 = \sigma\delta W + \left(\frac{d\Omega}{d\varpi} + \frac{2}{\varpi} \Omega - 2\Omega \frac{d\nu}{d\varpi} \right) \varpi e^{-\lambda} \delta U, \quad (67)$$

³ It is not difficult to realize that a constant specific angular momentum distribution yields the most compact tori among those having the same angular momentum at the cusp.

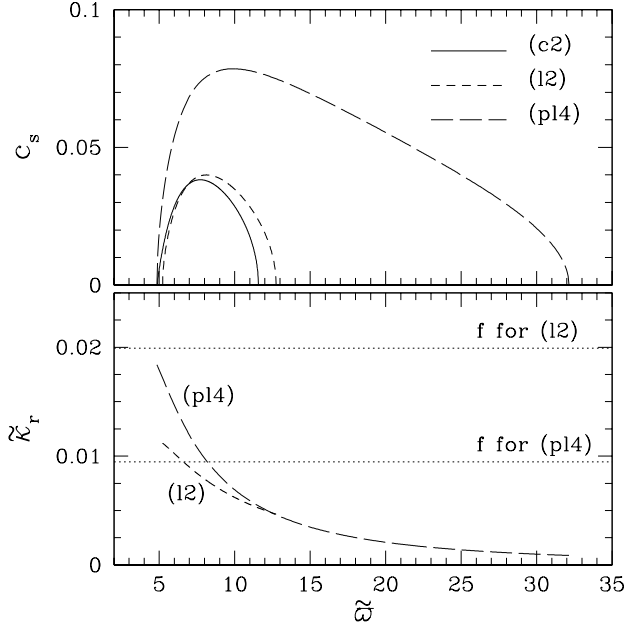


Figure 5. The upper panel shows the relativistic sound velocity for representative tori models having either a constant [solid line; model (c2)], a linear [short-dashed line; model (l2)] or a power-law [long-dashed line; model (pl4)] distribution of specific angular momentum. The lower panel, instead, shows the dimensionless radial epicyclic frequency for the three models shown in the upper panel, with the horizontal lines showing the fundamental frequencies for models (l2) and (pl4). All quantities are expressed in normalized units.

and can be solved adopting the same numerical technique used for the constant angular momentum models.

The upper panel of Figure 5 shows the relativistic sound velocity for representative unperturbed tori models having either a constant (solid line), a linear (dotted line) or a power-law (dashed line) distribution of specific angular momentum [The data refers to models (c2), (l2) and (pl4) of Table 1, respectively.]. Note that while all of the curves refer to models with a polytropic EOS, each curve does not depend on the value chosen for the polytropic constant k and hence on the mass of the disc (see Appendix B for a proof of this). The lower panel of Figure 5, on the other hand, shows the radial epicyclic frequency κ_r as calculated from expression (43) for the three models shown in the upper panel (we recall that $\kappa_r = 0$ when $\ell = \text{const.}$). The horizontal lines in the lower panel refer to the fundamental frequencies for models (l2) and (pl4) and their relative position with respect to the curves for κ_r will be important for the appearance of an evanescent-wave region in the inner parts of the torus (see the discussion below).

We have summarized in the different panels of Figure 7 the eigenfunctions for δQ , δU and δW for tori with a linear [panels (a)–(c)] and a power-law [panels (d)–(f)] distribution of specific angular momentum. The eigenfunctions refer, in particular, to models (l1) and (pl3) of Table 1 and are shown in the fundamental as well in the first three overtones. Similarly, are summarized in Table 2 also the eigenfrequencies computed for a number of tori with non-constant specific angular momentum.

A rapid analysis of the eigenfrequencies in Table 2 as well as of the eigenfunctions in the various panels of Figure 7 indicates that, overall, the results for non-constant distributions of specific angular momentum do not differ, at least qualitatively, from those

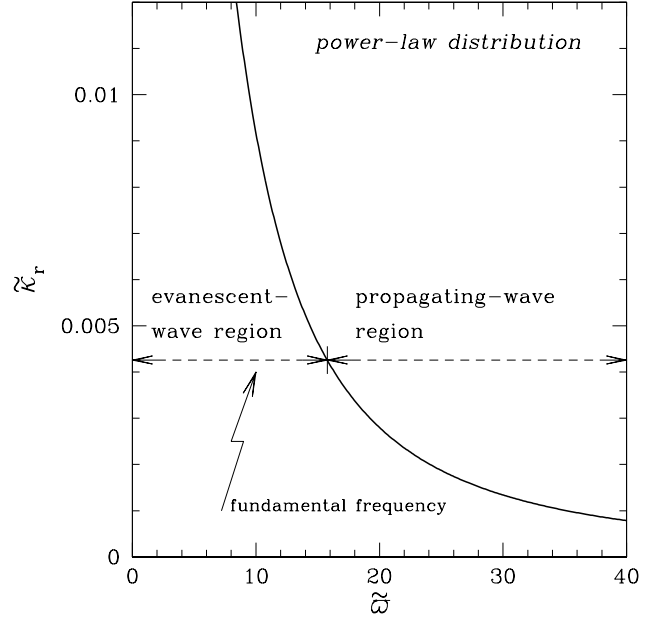


Figure 6. Schematic propagation diagram for a thick disc. The thick solid line shows the values of the relativistic radial epicyclic frequency κ_r in the inner regions of the disc, while the horizontal dashed line the value of the fundamental frequency f . The data is presented in normalized units and refers to model (pl2) of Table 1. See the main text for a discussion.

computed for constant distributions. Most importantly, the eigenfrequencies continue to appear in the simple sequence 2:3:4:..., at least for the lowest-order modes considered here.

This result may appear surprising in light of the fact that the radial epicyclic frequency defined by (43) does not vanish in the case of non-constant specific angular momentum distributions, so that the computed eigenfrequencies contain also a contribution coming from the inertial oscillations [cf. the dispersion relation (42)]. However, it is important to bear in mind that the p modes discussed here behave essentially as sound waves trapped inside the torus. As a result, while their absolute frequencies will be different when tori with different radial extensions are considered, the sequence in which they appear will basically follow the relation $\sigma_n = [(2+n)/2]f$.

The “universality” in which the lowest-order p -mode seem to appear has an interest of its own, but may also have important implications for the high frequency quasi-periodic oscillations observed in binaries containing a black hole candidate (Strohmayer 2001; Remillard et al., 2002). In at least three systems, in fact, the QPOs have been detected with relatively strong peaks that are in a harmonic ratio of small integers 1:2, 2:3, or 1:2:3 (Abramowicz, Kluzniak 2001), and a possible explanation of this phenomenology in terms of the oscillations of a geometrically thick, non-Keplerian disc of small radial extent orbits around the black hole will be presented in a separate paper (Rezzolla et al., 2003).

Before concluding this Section, we should underline an important qualitative difference that emerges when non-constant distributions of specific angular momentum are considered. This is related with the behaviour of the eigenfunctions for the radial velocity perturbation δU at the inner edge of the disc. A rapid comparison of Figure 2 with the corresponding panels (b) and (e) of Figure 7 shows that the eigenfunctions become vanishingly small

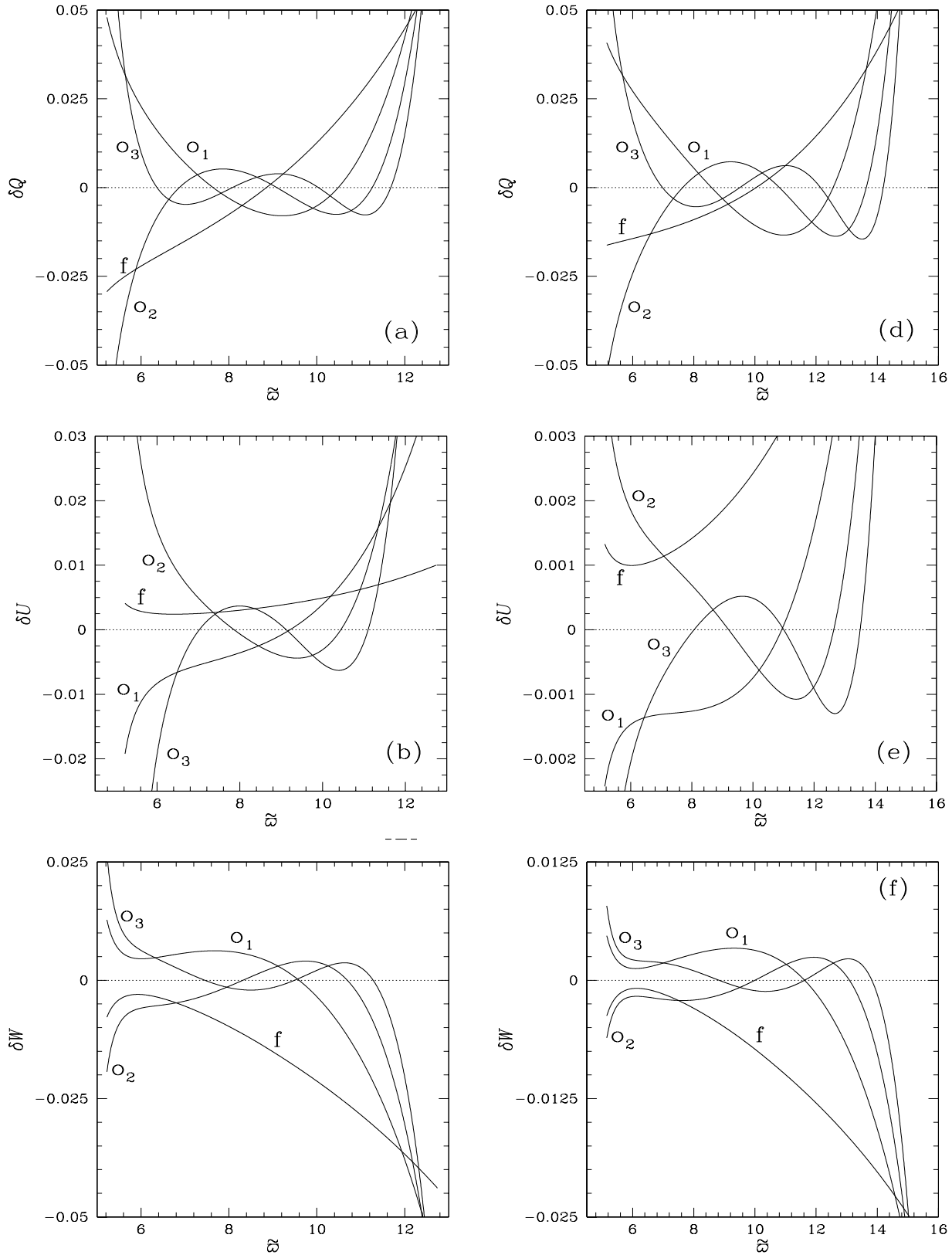


Figure 7. Eigenfunctions for $\delta Q = \delta P/(E + P)$, $\delta U = i\delta V^{\hat{\phi}}$, and $\delta W = \delta V^{\hat{\phi}}$ as a function of the radial coordinate for a tori with a “linear” [panels (a)–(c); model (11)] and a “power-law” [panels (d)–(f); model (pl3)] distribution of the specific angular momentum. While the units used on the vertical axes are arbitrary, it should be noted that the values on panel (e) are one order of magnitude smaller than the corresponding ones on panel (b). In all panels only the fundamental mode f and the first three overtones have been reported.

at the inner edge of the disc in the case of “power-law” distribution of specific angular momentum. This does not seem to be case for the behaviour at the outer edge, where the eigenfunctions maintain very large values. Similarly, this behaviour at the inner edge is not encountered with the other two distributions considered [note that the values on vertical axis of panel (e) are one order of magnitude smaller than the corresponding ones on panel (b) and in Figure 2].

A physical explanation for this behaviour can be found by comparing the behaviour of the radial epicyclic frequency curves for the different distributions of angular momentum. The lower panel of Figure 5, in particular, shows that the radial epicyclic frequency for both the linear and the “power-law” distributions of specific angular momentum are monotonically decreasing for increasing radii (This has been found to hold for all of the disc models considered here.). However, while the two frequencies tend to be comparable in the outer regions of the torus, they differ considerably in the inner regions, where the epicyclic frequency for a power-law distribution increases inward much more rapidly. More importantly, the epicyclic frequency is always *smaller* than the fundamental frequency for a torus with a linear distribution of angular momentum, while this is not the case for a power-law distribution (cf. Table 2).

In this latter case, then, there will be regions of the disc in which $\sigma^2 - \kappa_r^2 \sim k^2 c_s^2 < 0$ and thus where the amplitude of any acoustic wave is forced to be zero (Other modes, such as the g modes, can however exist in this region, in which they are actually trapped; Kato and Fukue, 1980). Such a region is referred to as an *evanescent-wave* region and effectively represents the part of the disc in which the centrifugal barrier produced by rotation makes the radial epicyclic frequency so high that all inward moving acoustic waves cannot propagate but are reflected back to larger radial positions. In those parts of the disc where the fundamental frequency is larger than the radial epicyclic one, on the other hand, $\sigma^2 - \kappa_r^2 > 0$, and sound waves can propagate undamped at least in a perfect fluid. Stated differently, the results found here indicate that, when acoustic waves are considered, the inner regions of the torus are of evanescent type for discs with a power-law distribution of angular momentum, while no evanescent region exists in a constant or in a linear distribution of specific angular momentum.

Finally, it is worth pointing out that the behaviour discussed above can be used to interpret some of the most recent results on the occurrence of the runaway instability (Font and Daigne 2002a, 2002b; Zanutti et al., 2003). In a series of relativistic hydrodynamics calculations of a torus orbiting and accreting onto a rotating black hole, in fact, Font and Daigne (2002b) have found that while tori with constant specific angular momentum distributions lead to a runaway instability, a slight outward increase as a power-law of the specific angular momentum, has a dramatic stabilizing effect, suppressing the instability completely. While this behaviour reflects a process which is fundamentally nonlinear, it is indeed consistent with the interpretation that the inner regions of thick discs prevent the inward propagation of perturbations and hence tend to suppress the accretion of mass onto the black hole. Because the runaway instability is fed by the changes in the spacetime produced by the mass accretion, a considerable reduction of the latter can be the cause of the suppression of the former. A more detailed investigation is necessary to validate this hypothesis.

8 CONCLUSIONS

We have presented the first investigations of the oscillation properties of relativistic, non-selfgravitating tori orbiting around a black hole. More precisely, we have here considered the axisymmetric oscillation modes of a geometrically thick disc constructed in a Schwarzschild spacetime. Like relativistic stars, relativistic tori are extended objects with non-trivial equilibrium configurations governed by the balance among gravitational, centrifugal and pressure forces. Unlike relativistic stars, however, the contributions coming from centrifugal forces are not small in relativistic tori and this amplifies the role of oscillations restored by centrifugal forces. This leads to oscillations properties that can be considerably different from those encountered in stars.

Because thick discs have angular momentum distributions that are intrinsically non-Keplerian, we have modeled them with a number of different distributions of specific angular momentum, which have been chosen to be either constant within the torus, or with a radial dependence being linear or a power-law. Furthermore, in order to keep the treatment as simple as possible and handle equations analytically whenever possible, we have built the models for the tori using vertically integrated and vertically averaged quantities.

Rather little is still known about the oscillation modes of relativistic tori and our approach to the problem has therefore progressed by steps. In particular, our first step has been that of considering the dispersion relation for acoustic waves propagating within these objects. We have done this firstly in a Newtonian framework in which equations are simpler and so is their physical interpretation. We have then extended the local analysis to a general relativistic framework and in particular to a Schwarzschild black hole spacetime. While a local analysis and the resulting dispersion relation is valid only for oscillations with wavelengths small when compared with the typical lengthscale in the tori, the ones derived here have been important to clarify the relation between the acoustic waves and the other waves that play a fundamental role in fluids orbiting in a central potential, i.e. inertial (or epicyclic) waves. In particular, it has been possible to show that, in general, both acoustic and inertial oscillations are present in the perturbations of thick discs and that the latter can be removed only in the special case of a constant distribution of specific angular momentum. This result, which was already known in Newtonian physics, has here been shown to hold also for extended relativistic fluid configurations. To the best of our knowledge this result has never been discussed in the literature before.

Going a step further and beyond a local analysis, we have used the same mathematical setup to perform a global analysis and determine both the eigenfunctions and the eigenfrequencies of the axisymmetric oscillations. Also in this case, the assumption of a vertically integrated equilibrium has simplified the eigenvalue problem considerably, translating it into a set of coupled ordinary differential equations which have been solved using standard techniques and for a number of different models for the tori. The modes found in this way correspond to the p modes of relativistic tori and are characterized by eigenfrequencies appearing in a simple sequence of small integers 2:3:4:..., at least for the first lower-order modes. This important feature does not depend on the distribution of angular momentum used to build the tori and basically reflects the fact that p modes are to be interpreted as sound waves trapped within the cavity represented by the confined torus.

The properties found here with a linear global analysis are in very good agreement with the numerical results found in the time

evolution of perturbed “toroidal neutron stars” having constant distributions of specific angular momentum (Zanotti et al., 2003). This agreement with fully nonlinear two-dimensional simulations provides convincing evidence that the assumption of a vertically integrated equilibrium has not subtracted important information from the present analysis.

A number of motivations are behind the investigations carried in this paper. Firstly, and as mentioned above, relativistic tori possess a rich variety of oscillation modes which are still essentially unexplored, in stark contrast with what is known (both in Newtonian and in relativistic regimes) about geometrically thin discs. In this respect, the present work was intended as a first investigation of the discoseismology of geometrically thick discs. Secondly, our analysis was aimed at interpreting and clarifying some of the results found by Zanotti et al. (2003), who had investigated numerically the dynamical response of massive tori to perturbations but had not been able to characterize all of the mode properties. Finally, by investigating the response of tori to perturbations, we intended to highlight possible connections between the oscillation modes of these objects and all those astrophysical scenarios in which geometrically thick discs may play an important role.

Some of the results discussed here could find application in more general contexts. One of such applications is offered by the quasi-periodic X-ray phenomenology observed in X-ray binary systems containing a black hole candidate (Strohmayer 2001; Remillard et al., 2002). In these systems, in fact, the X-ray emission is modulated quasi-periodically with power spectra having peaks in a harmonic ratio of small integers 1:2, 2:3, or 1:2:3 (Abramowicz and Kluzniak, 2001). While there are a number of possible explanations for this behaviour, it could be interpreted simply in terms of the p -mode oscillations of a geometrically thick, non-Keplerian disc of small radial extent orbiting around the black hole (Rezzolla et al., 2003). Another of such applications is offered by the runaway instability which has recently been considered by a number of authors (Font and Daigne 2002a, 2002b; Zanotti et al., 2003) through fully nonlinear numerical calculations. In particular, the numerical evidence that the instability can be suppressed if the torus has a distribution of angular momentum which is slightly increasing outwards, can be interpreted simply in terms of the behaviour of the eigenfunctions for the radial velocity perturbations, which become vanishingly small in the inner regions of the disc. This, in turn, is produced by the appearance of a region of evanescent-wave propagation in the inner regions of the torus that prevents the inward propagation of perturbations, reduces the accretion of mass onto the black hole, thus suppressing the instability.

As mentioned in the abstract, the present work represents the first of a series of papers aimed at a systematic investigation of the oscillation properties of relativistic tori. We are presently investigating extensions of the present approach in which the p modes are investigated both when the background spacetime is that of a Kerr black hole (Rezzolla & Yoshida, in preparation), and when deviations from axisymmetry are present. In addition to this, work is also in progress to extend the solution of the eigenvalue problem to a fully two-dimensional model for the torus. The results of these investigations will be presented in future papers.

ACKNOWLEDGMENTS

It is a pleasure to thank N. Andersson, O. Blaes, T. Font, W. Kluzniak, and J. Miller for many useful discussions. Financial support for this research has been provided by the MIUR and by the EU

Network Programme (Research Training Network Contract HPRN-CT-2000-00137). The computations were performed on the Beowulf Cluster for numerical relativity “*Albert100*”, at the University of Parma.

APPENDIX A: ON THE VALUES OF THE EIGENFREQUENCIES WHEN $L \rightarrow 0$

In the limit of vanishing torus sizes, $L \rightarrow 0$, all of the eigenfunctions can be assumed to have only a simple linear dependence on ϖ , i.e.

$$\delta U = a\varpi + b, \quad (\text{A1})$$

$$\delta W = c\varpi + d, \quad (\text{A2})$$

$$\delta Q = e\varpi + f, \quad (\text{A3})$$

where a, b, \dots, f are just constant coefficients. Using this ansatz in the system of perturbed equations (35)–(37), we obtain the following system of equations

$$\varpi[\sigma a + 2ce^{-\lambda}\Omega S(\varpi) + ikAe^{-\nu-\lambda}e] + \sigma b + 2de^{-\lambda}\Omega S(\varpi) + ikAe^{-\nu-\lambda}f = 0, \quad (\text{A4})$$

$$\varpi[\sigma c + ae^{-\lambda}H(\varpi)] + \sigma d + be^{-\lambda}H(\varpi) = 0, \quad (\text{A5})$$

$$\varpi \left[\sigma e + \frac{\Gamma P}{E + P} ae^{\nu-\lambda} ik \right] + \sigma f + \frac{\Gamma P}{E + P} e^{\nu-\lambda} ik b = 0, \quad (\text{A6})$$

where

$$H(\varpi) \equiv 2\Omega + \varpi \frac{d\Omega}{d\varpi} - 2\Omega\varpi \frac{d\nu}{d\varpi}, \quad (\text{A7})$$

$$S(\varpi) \equiv 1 + \frac{\varpi}{E + P} \frac{dP}{d\varpi}, \quad (\text{A8})$$

and where it is easy to realize that the radial epicyclic frequency is then simply given by [cf. eq. (43)]

$$\kappa_r^2 = 2e^{-2\lambda}\Omega H(\varpi)S(\varpi). \quad (\text{A9})$$

Each of the equations in the system (A4)–(A6) can be written symbolically as $\alpha_i\varpi + \beta_i = 0$, $i = 1, 2, 3$ with α_i and β_i being just shorthands for the longer expressions in (A4)–(A6). Furthermore, because each equation in of the (A4)–(A6) must hold for any ϖ , we need to impose that all of the coefficients α_i and β_i vanish simultaneously. This generates a system of six equations in the six

unknowns a, b, \dots, f

$$\sigma a + 2c\Omega e^{-\lambda} S(\varpi) + ikAe^{-\nu-\lambda} e = 0, \quad (\text{A10})$$

$$\sigma b + 2d\Omega e^{-\lambda} S(\varpi) + ikAe^{-\nu-\lambda} f = 0, \quad (\text{A11})$$

$$\sigma c + ae^{-\lambda} H(\varpi) = 0, \quad (\text{A12})$$

$$\sigma d + be^{-\lambda} H(\varpi) = 0, \quad (\text{A13})$$

$$\sigma e + \frac{\Gamma P}{E+P} e^{\nu-\lambda} ika = 0, \quad (\text{A14})$$

$$\sigma f + \frac{\Gamma P}{E+P} e^{\nu-\lambda} ikb = 0, \quad (\text{A15})$$

which, in matrix form, can be written as

$$\mathcal{A} \begin{pmatrix} a \\ b \\ \vdots \\ f \end{pmatrix} = 0. \quad (\text{A16})$$

A non-trivial solution to the system (A16) is possible if the determinant of the matrix \mathcal{A} vanishes and, after lengthy but straightforward calculations, this condition yields

$$\det(\mathcal{A}) = \sigma^2 \left[\sigma^2 - 2\Omega e^{-2\lambda} H(\varpi) S(\varpi) \right] \left[\sigma^2 - 2\Omega e^{-2\lambda} H(\varpi) S(\varpi) + \sigma \left(\frac{\Gamma P}{E+P} \right)^2 k^4 A^2 e^{-4\lambda} + 2 \frac{\Gamma P}{E+P} k^2 A e^{-2\lambda} \right] = 0 \quad (\text{A17})$$

Since $\Gamma P/E + P \sim c_s^2$, all of the terms proportional to this quantity can be neglected in (A17), which then reduces to

$$\sigma^2 \left[\sigma^2 - 2\Omega e^{-2\lambda} H(\varpi) S(\varpi) \right]^2 = 0. \quad (\text{A18})$$

A non-trivial solution of equation (A18) is then given by

$$\sigma^2 = 2\Omega e^{-2\lambda} H(\varpi) S(\varpi) = \kappa_r^2, \quad (\text{A19})$$

thus proving that the eigenfrequencies tend to the value of the epicyclic frequency in the limit of $L \rightarrow 0$.

APPENDIX B: ON THE SOUND SPEED IN ROTATING POLYTROPIC TORI

We here show that a *non-self gravitating, polytropic* fluid configuration orbiting in *hydrostatic equilibrium* around a Schwarzschild black hole has a sound velocity which is invariant under changes of the polytropic constant k . To prove this consider the equation of hydrostatic equilibrium (28) which, in the simplified metric (22), can be rewritten as

$$\frac{\partial \varpi p}{e+p} = -\frac{e^{2\nu} \partial \varpi \nu - \Omega^2 \varpi}{e^{2\nu} - \Omega^2 \varpi^2} = f(\varpi). \quad (\text{B1})$$

The right-hand-side of equation (B1) depends only on the kinematic and geometric properties of the disc, namely on the angular momentum distribution (through Ω) and on the external gravitational field of the central black hole (through ν). Both of these quantities depend on ϖ only.

Introducing the relation $\gamma = 1 + 1/n$, the polytropic EOS $p = k\rho^\gamma$ can also be written in terms of the Emden function $\Theta^n \equiv \rho$ as

$$p = k\Theta^{N+1}, \quad (\text{B2})$$

so that equation (B1) effectively becomes

$$\frac{\partial \varpi \psi}{1+\psi} = f(\varpi), \quad (\text{B3})$$

where we have defined $\psi \equiv k(n+1)\Theta$.

Equation (B3) can be integrated analytically to give

$$\psi(\varpi) = \mathcal{C} \exp \left[\int_{\varpi_{\text{in}}}^{\varpi} f(\varpi') d\varpi' \right] - 1, \quad (\text{B4})$$

where \mathcal{C} is an arbitrary constant.

The important result contained in equation (B4) is that ψ is a function of ϖ only and will not depend, therefore, on the specific value chosen for k . As a result, once γ (and thus n) is fixed, any transformation $K \rightarrow K\alpha$, where α is an arbitrary constant, must be accompanied by a corresponding transformation $\Theta \rightarrow \Theta/\alpha$. An important consequence of this is that all of the quantities given by p/ρ , $dp/d\rho$, p/e , dp/de are invariant under changes in k . Equally invariant is the sound speed defined as $c_s \equiv \sqrt{dp/de}$.

To appreciate the physical implications of this result, it is useful to recall that the polytropic constant plays here the role of determining the total rest-mass of the torus. Once the other parameters of the background model have been fixed (i.e. the distribution of angular momentum and the potential gap), in fact, the rest-mass of the torus is calculated from the integral

$$M_t \equiv \int_{\varpi_{\text{in}}}^{\varpi_{\text{out}}} 2\pi \varpi \Sigma u^t \varpi d\varpi. \quad (\text{B5})$$

As a consequence, different choices for k will yield tori with different density distributions Σ and hence rest-masses, while maintaining the same radial extension. The result contained in equation (B4) states, therefore, that it is possible to build tori with largely different rest-mass densities and yet have them all share the same sound velocity.

Two additional remarks are worth making. The first one is that while this result has been derived for a disc with a nonzero vertical extension, it applies also for a vertically integrated model. The second remark is that while we have been here concentrating on relativistic models, the same result can be shown to apply in Newtonian physics when the central black hole is replaced by a generic spherically symmetric gravitational potential.

REFERENCES

- Abramowicz, M. A., Calvani, M., Nobili, L., 1983, *Nature*, 302, 597
- Abramowicz, M.A., Kluzniak, W., 2001, *A&A*, 374, L19
- Blaes, O. M. 1985, *MNRAS*, 216, 553
- Cowling, T. G., 1941, *MNRAS*, 101, 367
- Cox, J. P., 1980, in “*The Theory of Stellar Pulsation*”, Princeton Univ. Press
- Davies, M. B., Benz, W., Piran, T., Thielemann, F. K., 1994 *ApJ*, 431, 742
- Font, J. A., Daigne, F., 2002a, *MNRAS*, 334, 383
- Font, J. A., Daigne, F., 2002b, *ApJ*, 581, L23
- Friedman, J. L., 1978, *Comm. Math. Phys.*, 62, 247

- Ipser, J. R., Lindblom, L., 1992, ApJ, 389, 392
- Kato, S., Fukue, J., 1980, PASJ, 32, 377
- Kato, S., Fukue, J., Mineshige, S., 1998, in *Black Hole Accretion Disks*, Kyoto University Press, Japan
- Kato S., 2001, PASJ, 53, 1
- Kojima Y., 1986, Prog. Theor. Phys., 75, L1464
- Kozłowski, M., Jaroszynski, M., Abramowicz, M. A., 1978, A&A, 63, 209
- Novikov, I., Thorne, K. S., 1973, in *Black Holes*, eds. B. de Witt and C. de Witt, Gordon and Breach, NY 491, 663
- Nowak, M. A., Wagoner, R. V., 1991, ApJ, 378, 656
- Nowak, M. A., Wagoner, R. V., 1992, ApJ, 393, 697
- Nowak, M. A., 1995, P.A.S.P., 718, 1207
- Okazaki, A. T., Kato, S., Fukue, J., 1987, PASJ, 39, 457
- Papaloizou, J. C. B., Pringle, J. E. 1984, MNRAS, 208, 721
- Papaloizou, J. C. B., Pringle, J. E. 1985, MNRAS, 213, 799
- Perez C. A., Silbergleit A. S., Wagoner R. V., Lehr D. E., 1997, ApJ, 476, 589
- Remillard, R.A., Munro, M.P., McClintock, J.E., Orosz, J.A., 2002, ApJ, 580, 1030
- Rezzolla, L., Yoshida, S'i., Maccarone, T. J., Zanotti, O., 2003 MNRAS, *in press*
- Rezzolla, L., Yoshida, S'i., 2003, *in preparation*
- Rodríguez M. O., Silbergleit A. S., Wagoner R. V., 2002, ApJ, 567, 1043
- Shu, F., 1992, in *The physics of Astrophysics, Vol 2, Gas dynamics*, University Science Books
- Silbergleit, A. S., Wagoner, R. V., Rodríguez, M., 2001, ApJ, 548, 335
- Stergioulas, N., Living Rev. Relativity 1, (1998), 8
- Strohmayer, T., 2001, ApJ, 552, L49
- Tassoul, J. L., 1978, in *Theory of Rotating Stars*, Princeton University Press
- Unno, W., Osaki, Y., Ando, H., Saio, H., Shibahashi, H., 1989, in *Nonradial Stellar Oscillations*, Tokyo University Press
- van der Klis, M., 2000, ARA&A, 38, 717
- Yoshida, S'i., Eriguchi, Y., 1995, ApJ, 438, 830
- Yoshida, S'i., Eriguchi, Y., 1997, ApJ, 490, 779
- Zanotti, O., Rezzolla, L., Font, J. A., 2003, MNRAS, 341, 832